Pcdp1 is a central apparatus protein that binds Ca^{2+}-calmodulin and regulates ciliary motility

Christen G. DiPetrillo and Elizabeth F. Smith

Department of Biological Sciences, Dartmouth College, Hanover, NH 03755

For all motile eukaryotic cilia and flagella, beating is regulated by changes in intraciliary calcium concentration. Although the mechanism for calcium regulation is not understood, numerous studies have shown that calmodulin (CaM) is a key axonemal calcium sensor. Using anti-CaM antibodies and *Chlamydomonas reinhardtii* axonemal extracts, we precipitated a complex that includes four polypeptides and that specifically interacts with CaM in high [Ca^{2+}]. One of the complex members, FAP221, is an orthologue of mammalian Pcdp1 (primary ciliary dyskinesia protein 1). Both FAP221 and mammalian Pcdp1 specifically bind CaM in high [Ca^{2+}]. Reduced expression of Pcdp1 complex members in *C. reinhardtii* results in failure of the C1d central pair projection to assemble and significant impairment of motility including uncoordinated bends, severely reduced beat frequency, and altered waveforms. These combined results reveal that the central pair Pcdp1 (FAP221) complex is essential for control of ciliary motility.

Introduction

Understanding how dynein is regulated to produce the waveforms typical of beating cilia and flagella is among the most pressing questions in the field of motility. These complex waveforms result from temporal and spatial regulation of dynein-driven microtubule sliding. In addition, virtually all motile cilia and flagella modulate their motility in response to changes in the intraciliary concentrations of the second messenger calcium. For example, in the presence of high calcium levels, sperm flagella and respiratory cilia increase their beat frequency (Brokaw et al., 1974; Verdugo, 1980), and flagella of *Chlamydomonas reinhardtii* switch from an asymmetric to a symmetric waveform (Bessen et al., 1980) (note: because the structures and polypeptides that comprise cilia and flagella are virtually identical, we use these two terms interchangeably).

Several calcium-binding proteins are components of the ciliary axoneme (for review see DiPetrillo and Smith, 2009). Our in vitro functional studies using axonemes isolated from wild-type and mutant *C. reinhardtii* cells provided evidence that calmodulin (CaM) is a key calcium sensor and that the central apparatus and radial spokes are integral components of the calcium signaling pathway (Smith, 2002; Dymek and Smith, 2007). Understanding the role of calcium and CaM in regulating dynein activity requires the identification and localization of CaM binding partners. Based on the large body of CaM literature (for review see Chin and Means, 2000), we hypothesized that CaM would exhibit differential affinity for particular interacting proteins in low versus high calcium conditions. In addition, we hypothesized that differential interaction of Ca^{2+}-CaM with specific axoneme components would play a role in altering dynein-driven microtubule sliding to control the size and shape of ciliary bends.

Previous investigators demonstrated that CaM is associated with the radial spoke stalk and that binding of CaM to particular stalk components is calcium sensitive (Yang et al., 2001; Patel-King et al., 2002, 2004). However, a substantial amount of axonemal CaM is not associated with the spokes. To identify additional CaM-interacting proteins, our laboratory used anti-CaM antibodies and extracts of axonemal proteins in immunoprecipitation experiments. In our first experiments we used low calcium buffer conditions and identified two distinct complexes. In addition to CaM, one complex contains five polypeptides including PF6; this complex most likely comprises the C1a central pair projection (Fig. 1 A; Wargo et al., 2005). Phenotypic analyses of C1-defective mutants (for review see Dutcher et al., 1984; Mitchell and Sale, 1999), as well as recent structural and functional studies (Smith, 2002; Wargo and Smith, 2003; Wargo

Correspondence to Elizabeth F. Smith: elizabeth.f.smith@dartmouth.edu

Abbreviations used in this paper: amiRNA, artificial microRNA; CaM, calmodulin; CSC, CaM- and spoke-associated complex; Pcdp1, primary ciliary dyskinesia protein 1; WT, wild type.

The Rockefeller University Press $30.00
J. Cell Biol. Vol. 189 No. 3 601–612
www.jcb.org/cgi/doi/10.1083/jcb.200912009

et al., 2004), have provided ample evidence to indicate that the C1 microtubule regulates motility. The flagella of the *C. reinhardtii pf6* mutant lack the C1a projection and are virtually paralyzed with only modest twitching (Dutcher et al., 1984; Rupp et al., 2001). In addition, our laboratory has shown that modulation of dynein activity on specific subsets of doublet microtubules in response to changes in calcium concentration is defective in *pf6* axonemes (Wargo et al., 2004). We predict that the CaM interactors associated with the C1a projection play a role in this modulation.

The second complex we identified, the CSC (CaM- and spoke-associated complex), is most likely localized near the base of the radial spokes (Dymek and Smith, 2007). This complex includes FAP91, a protein with significant sequence similarity to AAT-1, a protein identified in testis as an AKAP (A-kinase anchor protein)-binding protein. FAP91 directly interacts with CaM and the radial spoke protein RSP3 (an AKAP), located at the base of the spoke (Fig. 1 A). Addition of antibodies generated against FAP91 to mutant axonemes with reduced microtubule sliding velocity restores dynein activity to wild-type levels. These results strongly implicate the CSC in mediating regulatory signals between the radial spokes and dynein arms.

Based on the prediction that CaM has different axonemal binding partners in high calcium, we have now performed immunoprecipitation experiments in high calcium buffer. Here, we report the identification of a complex that includes four polypeptides in addition to CaM and that localizes to the C1d projection of the central apparatus. One member of the complex, FAP221, binds directly to CaM in a calcium-dependent manner and shares significant sequence identity with mammalian primary ciliary dyskinesia protein 1 (Pcdp1; Lee et al., 2008). Our functional and structural analyses of mutant strains with reduced expression of complex components provide direct evidence that this calcium-dependent CaM complex localizes to the C1d central pair projection and is essential for controlling ciliary beat frequency and waveform.

Results

Ca^{2+}-CaM binds to a 110-kD protein that is associated with the central apparatus

To identify potential calcium–calmodulin (Ca^{2+}-CaM) interactors, we performed a gel overlay assay using bacterially expressed *C. reinhardtii* CaM and axonemes isolated from wild-type (WT), *pf14*, and *pf18* cells. CaM bound to a protein of ~110 kD in the presence of high calcium buffer, but not in buffers with EGTA (Fig. 1 B). The 110-kD protein is present in WT and *pf14* axonemes, but appears lacking from *pf18* axonemes. These results suggest that the 110-kD protein is associated with the central apparatus. To isolate this protein, as well as to identify other Ca^{2+}-CaM interactors, we used a *C. reinhardtii*-specific anti-CaM antibody and extracted axonemal proteins in immunoprecipitation experiments (Fig. 1 C). These experiments were performed in the presence of either low or high calcium buffers and using extracts prepared from axonemes isolated from several *C. reinhardtii* mutants. The resulting precipitates were analyzed by SDS-PAGE using both high (not depicted) and low percentage polyacrylamide gels and silver stain for visualizing proteins (Fig. 1 C).

Four polypeptides, tentatively named HC1–4 and ranging in apparent molecular weight from 285 kD to 110 kD, were most consistently enriched in immunoprecipitates using high calcium buffer (Fig. 1 C, red asterisks). These four proteins are either lacking from or significantly reduced in precipitates of extracts isolated from the central apparatus defective mutants *pf18* and *pf16* (Fig. 1 C, blue asterisks). However, HC1–4 are precipitated from axonemal extracts isolated from *cpc1* and *pf6*. Based on the well-established structural defects for these mutants (Fig. 1 A), these results tentatively localize HC1–4 to the C1c or C1d projections of the central apparatus. CaM gel overlay analysis of precipitates confirmed that the 110-kD protein (HC4) was precipitated in high calcium buffer and only bound CaM under high calcium overlay conditions. These studies also revealed that HC4 was the only CaM interactor among HC1–4 (Fig. 1 D). These results suggest that HC4 corresponds to the 110-kD protein originally identified in gel overlay assays and that HC1–4 form a single complex with CaM.

Identification of HC1–4: FAP221 is the *C. reinhardtii* homologue of mammalian Pcdp1

To determine the identities of HC1–4, corresponding bands were excised from a polyacrylamide gel and subjected to mass spectrometry. Comparisons of the resulting peptides with the translated *C. reinhardtii* genome (version 3.0; http://genome.jgi-psf.org/Chlre3/Chlre3.home.html; (Merchant et al., 2007) revealed that HC1–4 correspond to four previously uncharacterized flagellar-associated proteins that were originally identified in the flagellar proteome (Pazour et al., 2005). The identities, in order of decreasing molecular weight, are FAP54, FAP46, FAP74, and FAP221 (Table I).

In database searches using the predicted amino acid sequences, putative homologues for all four proteins are only found in ciliated organisms. The top mammalian hit for each is shown in Table I and is a reciprocal best match. FAP54, FAP46, and FAP74 have no known functional domains and share sequence identity with predicted proteins of unknown function. However, FAP221 shares high amino acid sequence identity with the mouse protein, primary ciliary dyskinesia protein 1 (Pcdp1; Lee et al., 2008), particularly over two regions (Fig. 2 A). The first region spans aa 8–244 and shares 37% identity and 60% similarity with Pcdp1 (Fig. 2 A, red), whereas the second region spans aa 392–739 (Fig. 2 A, blue) and shares 33% similarity (for a comparison of Pcdp1 homologues from ciliated organisms, see the dendrogram in Fig. S1).

FAP221 has a predicted CaM binding site at aa 588–595 (see Calmodulin Target Database; http://calcium.uhnres.utoronto.ca/ctdb/ctdb/sequence.html). Pcdp1 contains two predicted CaM binding motifs. An IQ motif is located in the C terminus of the protein, and an uncharacterized CaM binding motif is located between aa 465–500. To confirm the predicted CaM binding site in FAP221 as well as determine if the two potential binding sites in Pcdp1 bind CaM, we bacterially

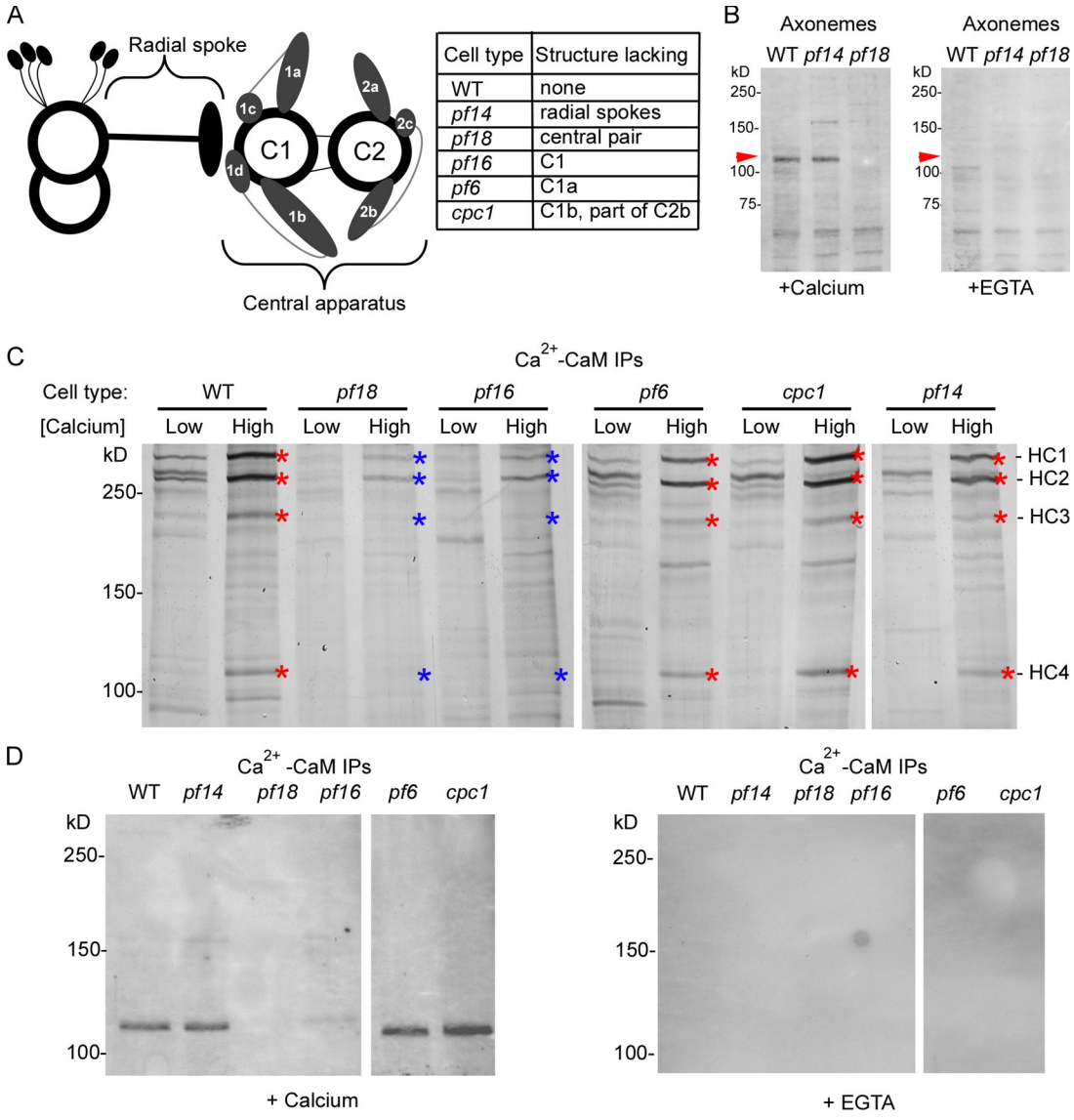

Figure 1. **Anti-CaM antibodies precipitate four polypeptides, one of which exhibits calcium-sensitive CaM binding.** (A) Diagram of the central apparatus and a single doublet microtubule with associated structures. Central pair projections are labeled. Inserted table lists WT and mutant strains used in this study along with the associated structural defects. (B) CaM gel overlay of WT, *pf14*, and *pf18* axonemes in high and low calcium conditions. CaM binds to a polypeptide of ~110 kD specifically in the presence of calcium (red arrowhead); this protein is missing from *pf18* axonemes. (C) Silver-stained gels of anti-CaM immunoprecipitation experiments (IPs) performed in low and high calcium buffers from axonemal extracts isolated from WT and mutant axonemes. Four polypeptides are precipitated that are highly enriched in high calcium IPs (HC1–4). These four polypeptides are missing or reduced from *pf18* and *pf16* anti-CaM IPs (blue asterisks) and are present at WT levels in *pf6*, *cpc1*, and *pf14* anti-CaM IPs (red asterisks). These results tentatively localize HC1–4 to the C1c or C1d projections of the central apparatus. (D) Corresponding CaM gel overlays of high calcium anti-CaM IPs from WT and mutant axonemal extracts. Only one of the precipitated proteins, HC4, exhibits calcium-sensitive CaM binding.

Table I. **Proteins precipitated with anti-CaM antibodies in high calcium buffers**

Protein	Flagellar proteome	Predicted MW	Predicted PI	Top mammalian hit	E value
HC1	FAP54	318,000	7.8	Predicted protein XP_001057963 (Rn)	9e-21
HC2	FAP46	289,000	6.6	Predicted protein XP_001092606 (Ma.m)	1e-14
HC3	FAP74	204,000	5.9	EAW56139 (Hs)	1e-79
HC4	FAP221	100,000	7.9	Primary ciliary dyskinesia protein 1 (Mu.m)	3e-51

Hs, *Homo sapien*; Ma.m, *Macaca mulatta*; Mu.m, *Mus musculus*; Rn, *Rattus norvegicus*.

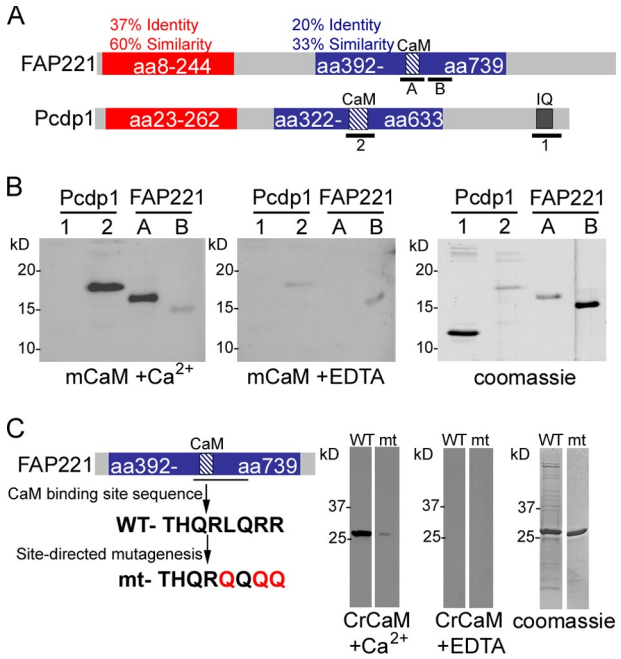

Figure 2. **Pcdp1 is the mammalian orthologue of FAP221.** (A) Diagram comparing the FAP221 and Pcdp1 protein coding sequences that share two major regions of identity. In the second region (shown in blue), both proteins have a predicted CaM-binding site (hatch marked region labeled "CaM"). Pcdp1 also has a predicted IQ motif at its C terminus (IQ). Regions that were expressed and used in the CaM gel overlay assay are marked with a black line; A and B for FAP221 and 1 and 2 for Pcdp1. (B) CaM gel overlay assay of FAP221 and Pcdp1 predicted CaM-binding regions. Overlays were performed with CaM from mouse (mCaM). The predicted CaM-binding regions shown in hatch marks only bind to CaM in the presence of high calcium. The predicted IQ motif at the C terminus of Pcdp1 does not bind to CaM under high or low calcium conditions. (C) Site-directed mutagenesis was used to alter three amino acids in the FAP221 CaM-binding site. Gel overlay analysis demonstrates the altered CaM-binding site no longer binds to *C. reinhardtii* CaM (CrCaM) in the presence of calcium.

expressed and purified the regions of interest for each protein and used them in gel overlay assays (Fig. 2 B). CaM preferentially binds to both FAP221 and Pcdp1 in the presence of high calcium. In addition, our data demonstrate that the uncharacterized motif in Pcdp1, and not the predicted IQ motif, binds Ca^{2+}-CaM.

The FAP221 CaM binding site was further confirmed by repeating the gel overlay assay using expressed protein fragments with either the WT CaM binding site or a CaM binding site in which three key amino acid changes were engineered (Fig. 2 C). The hydrophobic nature of leucine and basic property of arginine are predicted to aid in binding CaM to its interactor (see Calmodulin Target Database). Therefore, these amino acids were changed to the polar amino acid glutamine, which has a neutral charged side chain. CaM no longer bound to the mutagenized FAP221 fragment regardless of the calcium concentration. These results confirm the identification of the FAP221 CaM binding site.

FAP54, FAP46, FAP74, and FAP221 form a single complex

Our CaM immunoprecipitation results combined with CaM gel overlay suggested that FAP54, FAP46, FAP74, and FAP221 form a single complex with CaM. To characterize these proteins further, polyclonal antibodies were generated against FAP74 and FAP221 using synthetic peptides or purified bacterially expressed protein fragments, respectively (see Materials and methods). Both antibodies recognize a polypeptide of the predicted molecular weight on Western blots of wild-type axonemes; these polypeptides are lacking from *pf18* and reduced in *pf16* axonemes (Fig. 3 A). Importantly, anti-FAP74 and anti-FAP221 antibodies also recognize polypeptides of the predicted molecular weight in high calcium anti-CaM immunoprecipitates (Fig. 3 B).

Both anti-FAP221 and anti-FAP74 antibodies were used to precipitate proteins from axonemal extracts. The anti-FAP221 antibody proved ineffective for immunoprecipitation (not depicted). However, the anti-FAP74 antibodies precipitated all four members of the complex from WT axonemal extracts, as seen by silver stain (Fig. 3 C) and Western blots (for FAP74 and FAP221; unpublished data). Because we do not have antibodies generated against FAP54 and FAP46, the identities of the two highest molecular weight bands in our precipitates were confirmed by mass spectrometry. As expected, the four proteins are not precipitated from *pf18* axonemal extracts because FAP74 is missing from axonemes isolated from this mutant. We also analyzed the sedimentation profile of these polypeptides on sucrose gradients (Fig. 3 D). FAP74 and FAP221 cosediment on sucrose gradients at ~15S, consistent with our hypothesis. Immunoprecipitation of CaM from pooled gradient fractions revealed that both FAP54 and FAP46 also cosediment with FAP74 and FAP221 (Fig. 3 E). These results provide strong evidence that these four proteins form a single complex.

The Ca^{2+}-CaM interacting complex localizes to C1d and is required for wild-type motility

Searches of the *C. reinhardtii* sequence database and genetic maps revealed that no previously indentified mutations mapped near to any of the genes encoding FAP46, 54, 74, or 221. Therefore, no mutants are currently available for any of the complex members. Because targeted gene disruption is not yet possible in *C. reinhardtii*, we used an artificial microRNA (amiRNA) approach to reduce gene expression of complex components and thus gain additional information about their localization and function. This technique takes advantage of the cell's own microRNAs that function to regulate endogenous gene expression (Fig. 4 A). Gene-specific amiRNA vectors were constructed as described in Molnar et al. (2009) and transformed into WT *C. reinhardtii* cells (Kindle, 1990). After selection of transformants on paromomycin, we screened for abnormal swimming phenotypes. Flagella were isolated from transformants with swimming defects and assessed for reduced protein expression by Western blot. A total of 960 transformants were picked from two transformations. Of these, 80 transformants had apparent swimming defects and 34 of these were screened for the presence of FAP74 in isolated flagella. 25 screened transformants had reduced amounts of FAP74 protein compared with WT based on densitometry of Western blots.

For cells that were transformed with amiRNA vectors designed to knock down expression of FAP74, three transformants,

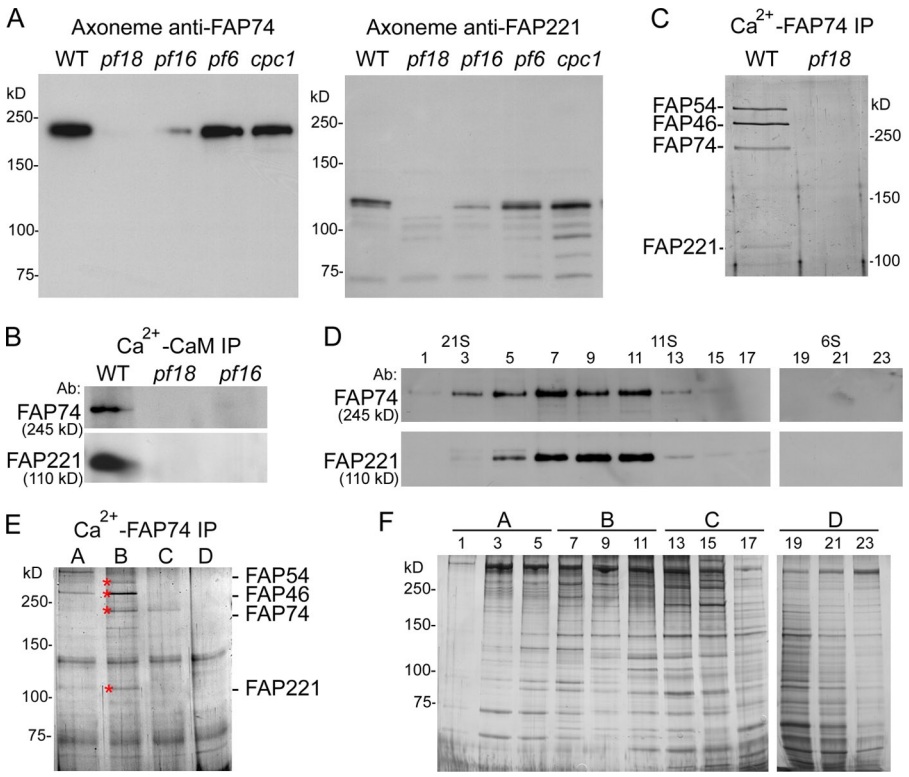

Figure 3. **FAP54, FAP46, FAP74, and FAP221 form a single complex.** (A) Western blots of isolated axonemes. FAP74 and FAP221 antibodies recognize proteins of the correct molecular weight and that are missing or reduced from *pf18* and *pf16*, but are present in WT, *pf6*, and *cpc1* axonemes. (B) These proteins are also present in anti-CaM IPs using WT axonemal extracts but not *pf18* and *pf16* extracts. (C) Silver-stained gel of high calcium anti-FAP74 IPs from WT and *pf18* NaCl axonemal extracts. All four proteins coprecipitate from WT extracts. The identities of FAP74 and FAP221 were confirmed by Western blot (not depicted). The identities of FAP54 and FAP46 were confirmed by mass spectrometry. (D) Western blots of WT axonemal extracts fractionated on a 5–20% sucrose gradient. FAP74 and FAP221 cosediment at ~15S. (E) Silver-stained gel of high calcium anti-FAP74 IPs from pooled sucrose gradient fractions (see F). All four members of the complex coprecipitate from pool B (fractions 7–11), and not from pools A, C, or D. (F) Silver-stained gel of WT axonemal extracts fractionated on a 5–20% sucrose gradient. Odd fractions were pooled together in designated groups A–D and used in high calcium anti-FAP74 IPs shown in E. These data support the conclusion that all four proteins form a single complex.

1G11, 2D4, and 7A4, from two independent transformation experiments showed the most significant reduction of FAP74 protein in flagella (Fig. 4 B) and were selected for further analysis. Importantly, unlike many procedures we have tried for RNAi-mediated knockdown of protein expression in *C. reinhardtii*, protein expression in these mutants appears to be stably reduced after many passages of cell cultures. We confirmed reduction of FAP74 expression by Northern blot (Fig. S2).

Flagella isolated from strain 1G11 appear to nearly completely lack FAP74 by Western blot, whereas densitometry analysis shows flagella isolated from strains 2D4 and 7A4 have an 87 and 78% reduction, respectively, of FAP74 compared with wild-type (Fig. 4 B). Interestingly, FAP221 still assembles into flagella of these mutant axonemes at apparently wild-type levels. However, immunoprecipitation of Ca^{2+}-CaM from extracts isolated from mutant extracts failed to precipitate FAP221 (Fig. 4 C). Silver-stained gels of the resulting precipitates also reveal that FAP54 and FAP46 are absent or severely reduced in precipitates from these strains (Fig. 4 C). In the absence of antibodies generated against FAP54 and FAP46, it is unknown whether they fail to assemble in transformants. However, our results indicate that the interactions of the polypeptides in this complex with Ca^{2+}-CaM and potentially with each other have been severely disrupted.

To determine if any structural defects result from reduced expression of FAP74, we prepared axonemes from 1G11, 2D4, and 7A4 for transmission electron microscopy. Transverse sections of axonemes isolated from each of these mutants revealed that the C1d projection of the central apparatus, as well as the sheath connecting the C1d and C1b projection, are either lacking or significantly reduced (Fig. 4 D, arrow). In the absence of the C1d projection, a space is seen between the radial spoke heads and central apparatus (Fig. 4 D, arrowhead). To ensure that we distinguish the central pair projections from the radial spoke heads, we generated double mutants with reduced FAP74 expression in combination with the *pf14* (radial spokeless) mutation. In the absence of the radial spokes, the defect in the C1d projection and sheath is easily recognized (Fig. 4, D and E).

As noted above, the FAP74-amiRNA mutants were selected among transformants for their altered motility. Using phase optics, 1G11, 2D4, and 7A4 cells appear to move significantly slower than wild-type with uncoordinated flagellar beating. Because the ability to phototax requires that flagella respond appropriately to increases in intraflagellar calcium, we used a simple phototaxis assay to test whether these strains retained the ability to phototax (see Materials and methods). All knockdown strains are capable of phototaxis. However, for strain 1G11 it took several hours for half of the cells to photo-accumulate. This result is most likely due to their motility defect rather than a defect in the ability to phototax.

To analyze flagellar beating of these strains quantitatively we used high speed video capture of swimming cells (see Materials and methods and Videos 1–4). All three strains showed significant reduction in swimming velocity compared with wild-type (Table II). 1G11 and 2D4 had velocities of approximately one-fourth of wild type, whereas swimming velocities of 7A4 were approximately one-half of wild type. Importantly, we were only able to measure swimming velocity for a fraction of the cells. In strain 1G11 only 29% of the cells were swimming. For 40% of cells, their flagella were either twitchy or one flagellum was paralyzed; these cells were unable

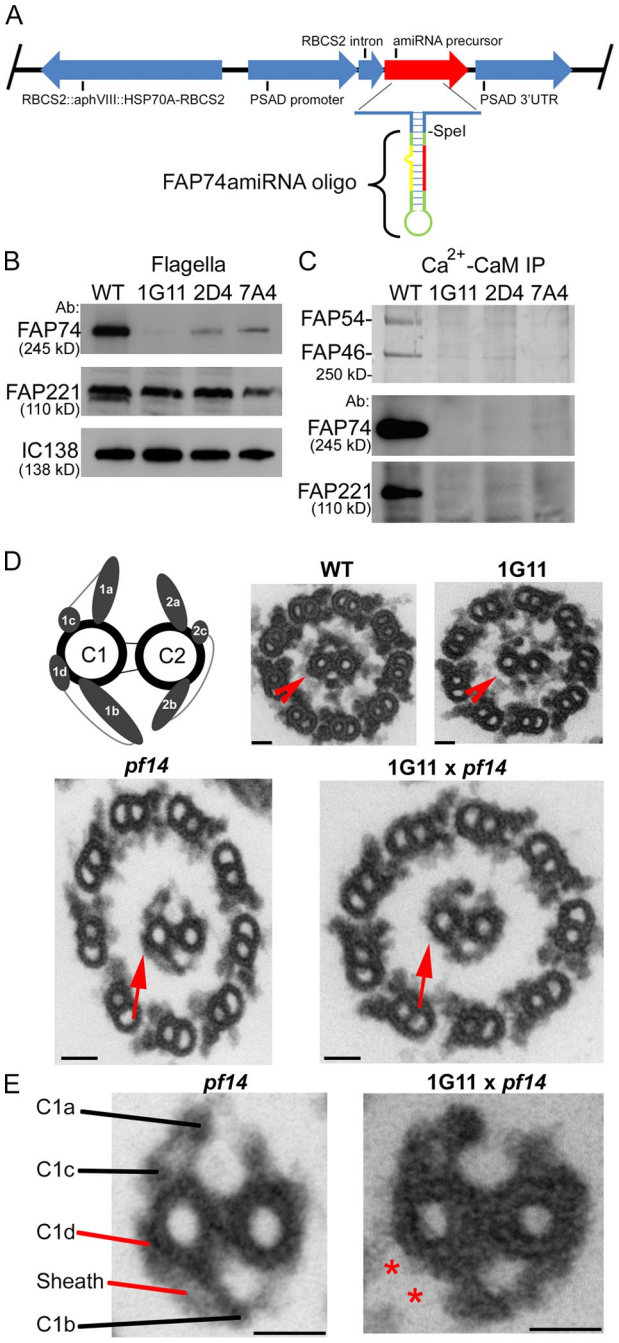

Figure 4. **Mutants with reduced expression of FAP74 lack the C1d central pair projection.** (A) Diagram of FAP74 artificial miRNA construct. (B) Western blot of WT and mutant flagella showing that FAP74 amiRNA transformants 1G11, 2D4, and 7A4 have reduced levels of FAP74. FAP221 levels are not reduced in these mutants. IC138 is a dynein intermediate chain used as a loading control. (C) Top panel is a silver-stained gel of high calcium anti-CaM IPs from axonemal extracts. Reduced amounts of FAP54 and FAP46 are immunoprecipitated from 1G11, 2D4, and 7A4 axonemal extracts compared with WT. Bottom panels are anti-FAP74 and anti-FAP221 Western blots of high calcium anti-CaM IPs showing that FAP74 and FAP221 are not precipitated from FAP74ami transformants. (D) Diagram shows the identities of the central pair projections. Electron micrographs of transverse sections of WT, 1G11, *pf14*, and 1G11,*pf14* mutant axonemes. (E) Enlarged view of the central apparatus from *pf14* and 1G11,*pf14* double-mutant axonemes. All micrographs are oriented with the axoneme viewed proximal to distal with the bar representing 25 nm; the C1 central microtubule in all images is to the left. The 1G11 and 1G11,*pf14* axonemes lack the C1d density and the sheath connecting C1d to C1b (marked by red arrows and asterisks).

to initiate a productive effective stroke to propel themselves through the media and often tumbled in circles. The remaining 31% of cells had paralyzed flagella.

Much of the reduction in swimming speed could be accounted for by a reduction in beat frequency. The average beat frequencies of 1G11, 2D4, and 7A4 are significantly reduced compared with wild type, with 1G11 beating at ∼30% of wild-type frequency (Table II). The magnitude of the reduction of beat frequency and swimming velocity roughly correlates with the amount of reduction of FAP74 expression with the greatest reduction observed for 1G11 in which FAP74 appears nearly absent in isolated axonemes. Upon close inspection of individual flagella, the reduction in beat frequency appears to be due in large part to stalling after the recovery stroke; the cells are defective in the ability to initiate the effective stroke.

To qualitatively evaluate beating in mutant strains we analyzed images from high speed video recordings. The still images in Fig. 5 illustrate the uncoordinated nature of flagellar motility for 1G11 compared with wild type (compare Video 1 with Videos 2–4). In these images and the corresponding traces, the flagella spend more time in the "hands-up" position before initiating an effective stroke. In some cases, the two flagella alternate bending (Fig. 5 B). In addition, for some cells one flagellum beats at one-quarter the frequency of the other flagellum (Fig. 5 C). To determine if the difference in beat frequency between the two flagella is a general feature of these mutants, we plotted the distribution of beat frequencies for a given population (unpublished data). We predicted that if this difference were a general feature of the population, we would observe a bimodal distribution of frequencies. For all three mutant strains, the distribution was normal. Therefore, this difference in beat frequency for the two flagella is not a general feature of these mutants.

For the FAP74ami transformants that are motile, we tested their ability to switch to a symmetric waveform in response to an increase in illumination (see Videos 5 and 6). All FAP74ami transformants were defective in their ability to switch waveform, with the greatest deficiency observed for strain 1G11. In this strain, only 4% of swimming cells were able to switch waveform. Interestingly, of the cells that switched to a symmetric waveform, the beat frequency of the symmetric waveform was not as severely reduced as the beat frequency for the asymmetric waveform (Table II). For example, there is a 70% decrease in the asymmetric beat frequency of 1G11 compared with WT, but only a 22% decrease in the symmetric beat frequency.

Discussion

Our previous in vitro functional studies of dynein-driven microtubule sliding using isolated axonemes demonstrated that CaM anchored to the axoneme is a key calcium sensor and that the central apparatus and radial spokes are integral elements of the calcium signaling pathway (Smith, 2002; Wargo et al., 2004; Dymek and Smith, 2007). Three different CaM-interacting protein complexes have been localized to these structures: RSP2, which localizes to the radial spoke stalk (Yang et al., 2001;

Table II. **FAP74ami mutant analysis**

Strain	Percent FAP74	Percent swimming (*n*)	Swimming velocity (μm/s) ± SEM (*n*)	Asymmetric beat freq (Hz) ± SEM (*n*)	Percent able to switch waveform (*n*)	Symmetric beat freq (Hz) ± SEM (*n*)
WT	100%	83% (281)	119 ± 7.9 (10)	50 ± 1.0 (77)	100% (91)	76 ± 3.2 (26)
1G11	1%	29% (146)	34 ± 2.3 (40)	15 ± 0.9 (90)	4% (91)	59 ± 4.5 (12)
2D4	13%	50% (354)	32 ± 1.3 (92)	17 ± 0.7 (116)	22% (104)	52 ± 2.3 (27)
7A4	22%	64% (133)	67 ± 3.5 (67)	24 ± 1.0 (122)	57% (49)	64 ± 2.7 (33)

Patel-King et al., 2002, 2004); FAP91, a component of the CSC, which tentatively localizes to the base of the spoke (Dymek and Smith, 2007); and FAP101, a component of the PF6 complex that localizes to the C1a central pair projection (Wargo et al., 2005). Here, we report the discovery of a protein complex that interacts with Ca^{2+}-CaM and localizes to the C1d projection of the central apparatus. The complex includes Pcdp1 and is required for wild-type motility. Our results provide the first assignment of polypeptides to the C1d central projection, and establish a definitive and essential role for this complex in regulating motility.

FAP54, 46, 74, and 221 form a single complex that exhibits calcium-sensitive CaM binding

Both our immunoprecipitation results and the sedimentation profile on sucrose density gradients support the conclusion that FAP54, 46, 74, and 221 form a single complex. All four polypeptides coprecipitate using either anti-CaM antibodies or anti-FAP74 antibodies, and all cosediment on sucrose gradients. Gel overlay assays of either immunoprecipitates or expressed proteins confirm that FAP221 is the only CaM interactor among these four polypeptides. In addition, the interaction of FAP221

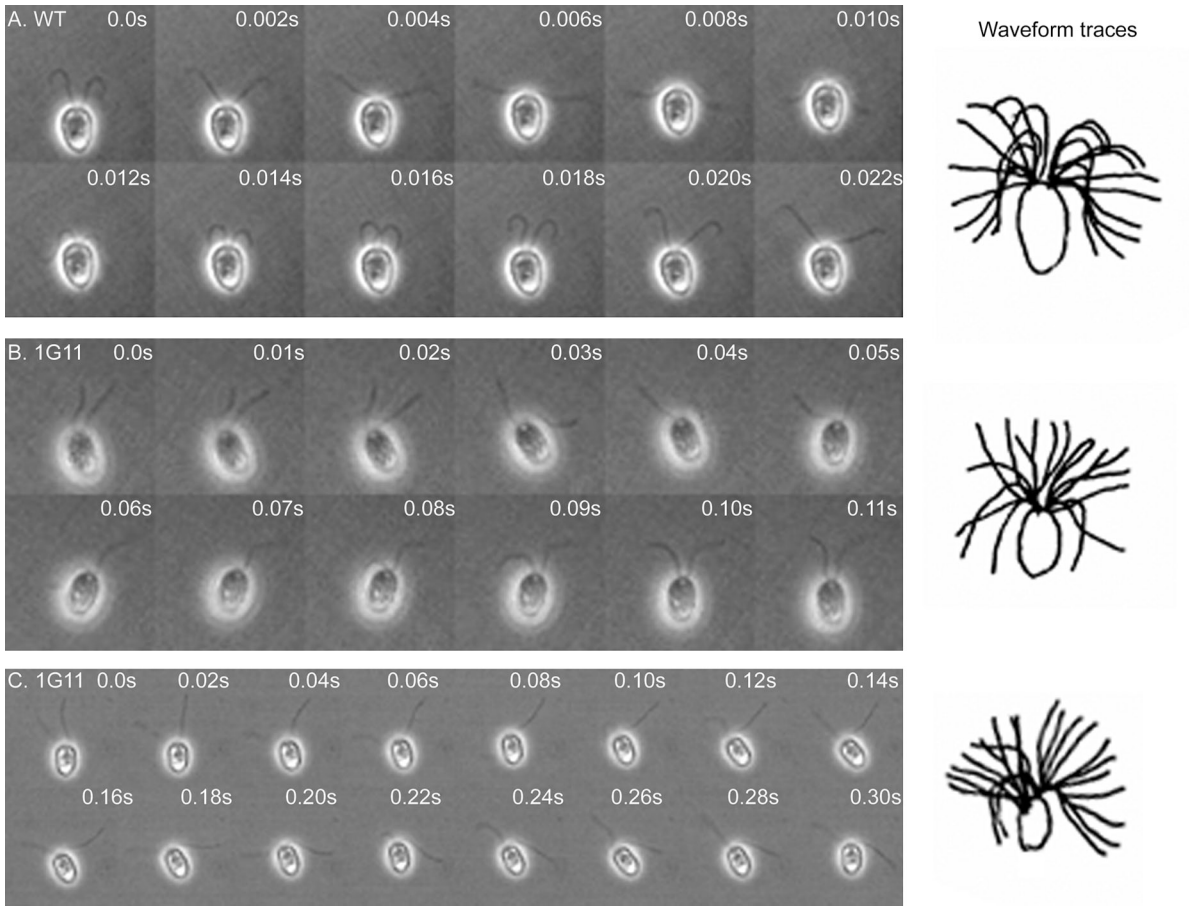

Figure 5. **FAP74ami transformants have slow and uncoordinated flagella with abnormal waveforms.** Montage of sequential frames from high speed recordings. Elapsed time in seconds is denoted on each frame. (A) WT cell displaying normal waveforms of two coordinated flagella (see Video 1). (B) 1G11 cell displaying uncoordinated flagellar movements. The right flagellum beats first, followed by the left flagellum. The corresponding waveform traces show an incomplete effective stroke and the lack of a normal recovery stroke (see Video 2). (C) 1G11 cell displaying uncoordinated flagella. The left flagellum completes two beats in the same time the right flagellum completes one effective stroke. The waveform traces also show the failure of the left flagellum to complete an effective stroke before beginning the recovery stroke. Examples of FAP74ami transformants 2D4 and 7A4 swimming can be seen in Videos 3 and 4, respectively.

with CaM is calcium sensitive and only occurs in the presence of high calcium.

Given that none of the four proteins precipitate from central apparatus defective mutants using anti-FAP74 antibodies, we concluded that these four polypeptides form a complex that is localized to the central apparatus. In analyses of anti-CaM immunoprecipitates from mutants that completely lack the central apparatus (*pf18*), FAP74 and FAP221 appear to be completely missing. However, FAP54 and FAP46 are present, albeit in significantly reduced amounts. Given the large size of FAP54 and FAP46 and the fact that they do not interact with CaM, it is possible that FAP221 is present in the precipitates at levels too low to detect by silver stain or gel overlay. Alternatively, FAP54 and FAP46 may bind to an additional Ca^{2+}-CaM interactor that localizes to an axonemal structure other than the central apparatus. To explore this possibility will require the generation of antibodies against FAP54 and FAP46.

FAP221 is the *C. reinhardtii* orthologue of Pcdp1 and localizes to C1d

FAP221 shares high amino acid sequence identity with mouse Pcdp1. Pcdp1, or primary ciliary dyskinesia protein 1, is a protein that when mutated in mice causes many of the same phenotypes observed in PCD, including hydrocephalus, respiratory defects (sinusitis), and male infertility (Lee et al., 2008). In particular genetic backgrounds, homozygous mutant mice die perinatally from hydrocephalus. In other genetic backgrounds the male mice are infertile, producing sperm with no visible flagella. Interestingly, in these mice cells of the respiratory tract do produce cilia; however, they beat with reduced frequency and exhibit an abnormal accumulation of mucus in their sinuses.

Lee et al. (2008) reported that there was no *C. reinhardtii* homologue for Pcdp1. However, they most likely searched the *C. reinhardtii* genome database for predicted coding sequences. In our studies, we discovered that the intron–exon prediction for FAP221 in the *C. reinhardtii* genome database was incorrect. Once the correct coding sequence was determined, the high degree of similarity between Pcdp1 and FAP221 was immediately obvious. Using this predicted amino acid sequence, we have also shown that apparent Pcdp1 homologues exist in all ciliated organisms (Fig. S1).

In addition to sharing significant sequence similarity, we demonstrated that both FAP221 and Pcdp1 are CaM-binding proteins and that the CaM binding domains appear to occur within the same region for each polypeptide. We have also shown that CaM binding for each of these polypeptides is calcium sensitive. Taken together with the functional data discussed below, FAP221 appears to be truly orthologous to Pcdp1.

The structural analyses of respiratory cilia in mutant mice by Lee et al. (2008) did not reveal any defects associated with the axoneme. However, reduced expression of the FAP74 member of the *C. reinhardtii* complex results in the absence of the C1d projection of the central apparatus. Therefore, this complex most likely localizes to C1d. Given the difficulty in preserving and staining axoneme structure within mammalian respiratory cilia, it is not surprising that these investigators were unable to discern such a distinct structural defect. Remarkably, based on the observed motility defect of mutant mice in comparison with the motility defects observed for central apparatus defective *C. reinhardtii* mutants, such as those that lack Hydin (Lechtreck and Witman, 2007; Lechtreck et al., 2008), Lee et al. (2008) suggested in their Discussion that Pcdp1 localizes to the central apparatus. Our results clearly demonstrate that their hypothesis was in fact correct.

Pcdp1–FAP221 is required for normal ciliary motility

Given that Pcdp1–FAP221 is a Ca^{2+}-CaM interactor, we predicted that this protein is involved in calcium-induced changes in motility. Mammalian sperm respond to increases in intraflagellar calcium by hyperactivation. Homozygous *pcdp1* mutants fail to assemble sperm flagella; therefore, it is not known whether this complex is involved in hyperactivation. This observation suggests that Pcdp1 in mammals also plays a role in flagellar assembly during spermatogenesis. Mammalian airway cilia respond to increases in calcium by increasing beat frequency. Mutant homozygous mice that lack Pcdp1 assemble airway cilia with reduced beat frequency (Lee et al., 2008). However, it is unknown if airway cilia from these mice also have altered waveforms or respond to changes in intracellular calcium concentration.

Although we have been unable to reduce expression of *C. reinhardtii* Pcdp1–FAP221, we have knocked down expression of the FAP221-interacting protein, FAP74. In these mutants FAP221 still assembles into flagella; however, its interaction with CaM is lost and the two other complex members FAP54 and FAP46 fail to either assemble or interact with FAP221. This defect results in the loss of the C1d projection. Using a variety of structural and biochemical approaches, all other axonemal components appear to be fully assembled. What is remarkable is that this small structural defect disrupts several fundamental features of motility. For the most significant knockdown of expression, only 29% of cells are swimming and their beat frequency is reduced to 30% of wild type. Flagella from these cells are uncoordinated, with defects in propagating bends and switching between effective and recovery strokes. Such a defect in switching has also been observed for *C. reinhardtii* mutants with reduced expression of Hydin (Lechtreck and Witman, 2007). Of the cells that have motile flagella, only 4% are able to switch between asymmetric (ciliary) and symmetric (flagellar) waveforms, a calcium-induced motility response. These results provide strong evidence that the Pcdp1–FAP221 complex not only plays a role in calcium regulation of motility, but also in control of normal wild-type beating.

As mentioned above, the loss of Pcdp1 from mutant mice results in slightly reduced beat frequency, yet the mice die perinatally of hydrocephalus. In *C. reinhardtii*, we have shown that reduced expression of the FAP221 complex member, FAP74, results in severely reduced beat frequency and altered waveforms. There are several possibilities to explain this difference in ciliary phenotype. First, it is not known if the cilia from *pcdp1* mutant mice have altered waveforms. The reduction in beat frequency seen in mutant mice most likely does not

account for the severe hydrocephalus and sinusitis. Therefore, it seems probable that there are additional defects in ciliary motility that are difficult to observe by video microscopy. Second, it is not known whether other components of the Pcdp1 complex assemble in *pcdp1* mutant mice. Reduced expression of FAP74 may result in a more significant structural and functional defect than knockout of *Pcdp1*–FAP221. Finally, these differences may be organism specific. As noted, *pcdp1* mutant mice assemble respiratory cilia but fail to assemble sperm flagella. Therefore, certain functions of Pcdp1–FAP221 may be unique to multicellular organisms.

A mechanism for Pcdp1–FAP221 function

The central apparatus is the home of many proteins known to be important for normal flagellar motility and function (for review see Mitchell, 2009). Although several studies using altered buffer conditions and low ATP concentrations have demonstrated that the radial spokes and central apparatus are not absolutely required for motility and waveform conversion (Omoto et al., 1996; Frey et al., 1997; Wakabayashi et al., 1997; Yagi and Kamiya, 2000), analysis of mutants in a variety of organisms demonstrate that these structures are required for normal motility in physiological conditions. Additional studies using combined functional and structural approaches support the hypothesis that calcium-induced changes in waveform affect dynein activity on specific doublet microtubules by a mechanism possibly involving orientation of the central pair (Yoshimura and Shingyoji, 1999; Bannai et al., 2000; Nakano et al., 2003; Wargo and Smith, 2003; Mitchell and Nakatsugawa, 2004; Hayashi and Shingyoji, 2009). The simplest model that can be derived from these analyses is that the central pair/radial spoke system acts as a signal transducer for controlling the size and shape of ciliary bends and for modifying motility in response to specific signals (for review see Smith and Yang, 2004). Given that such a small structural defect, such as the lack of C1d, resulted in such a significant defect in motility, we predict that the C1d projection is essential for the central pair/radial spoke interactions that are required for coordinated and regulated microtubule sliding.

Our working hypothesis is that these protein complexes act as molecular switches that alternate between CaM-associated and -dissociated states, depending on the concentration of intraciliary calcium. For example, the PF6 complex localizes to the C1a projection and binds to CaM in the presence of low calcium (Wargo et al., 2005). The FAP221-containing complex likely localizes to the C1d projection and binds CaM in the presence of high calcium. We postulate that the altered association of CaM with these complexes potentially alters the interaction of the central pair projections with the radial spoke heads to ultimately regulate dynein activity.

One of the most surprising discoveries in the past five to ten years is the number of diverse human diseases that result from defects in ciliary assembly and/or motility, so-called "ciliopathies" (for review see Badano et al., 2006; Sharma et al., 2008; Nigg and Raff, 2009). Defects in motility may result in impaired fertility, respiratory distress, and/or randomization of the left–right body axis. To date, mutations in *PCDP1* in humans have not been identified. Based on the mutant mouse phenotype, it is possible that mutations in *Pcdp1* as well as other ciliary proteins required for motility are either lethal or result in phenotypes not recognized as PCD in humans. Work in model organisms such as mice and *C. reinhardtii* will continue to provide important insights into the molecular mechanism of wild-type ciliary motility, and the defects that result in primary cilia dyskinesia.

Materials and methods

Strains and cell culture

C. reinhardtii strain A54-e18 (nit1-1, ac17, sr1, mt+) has wild-type motility and was obtained from Paul Lefebvre (University of Minnesota, St. Paul, MN), and the *cpc1-2* strain was from David Mitchell (SUNY Upstate Medical University, Syracuse, NY). The strains *pf16*, *pf6-2*, *pf14*, and *pf18* were obtained from the *Chlamydomonas* Genetics Center (Duke University, Durham, NC). Cells were grown in constant light in TAP media (Gorman and Levine, 1965). For electron microscopy analysis (see below), FAP74ami transformant 1G11 was mated with radial spokeless mutant *pf14*. Double mutant 1G11,*pf14* was selected from nonparental ditype tetrads and confirmed by Western blot (see below).

Axoneme isolation, protein extraction, sucrose gradient fractionation, and immunoprecipitation

Axonemes were isolated and extracted as described previously (Dymek and Smith, 2007) with the following modifications. KI extraction after NaCl extraction was not performed. NaCl extracts using 0.6M NaCl were prepared for all experiments using axonemal extracts. For some experiments, the clarified extracts were loaded onto 5–20% sucrose gradients prepared in NaLow and subjected to ultracentrifugation at 35,000 rpm for 16 h in a SW41Ti rotor (Beckman Coulter). Fractions (0.5 ml) were collected from the bottom of the tube and prepared for SDS-PAGE. For experiments performed in the presence of High Ca^{2+}, NaLow and NaHigh were both modified to contain 1.0 mM $CaCl_2$ and EDTA was omitted.

Immunoprecipitation was performed as described previously (Dymek and Smith, 2007) with the following modifications. 70 µg of anti-CaM or anti-FAP74 (N-terminal) affinity-purified antibodies was used. TBS-T (150 mM NaCl, 50 mM Tris-HCl, pH 7.4, 0.5 mM EDTA, and 0.2% sodium azide) was prepared with or without 1 mM $CaCl_2$. When calcium was present, EDTA was omitted.

Cloning and expression of *C. reinhardtii* FAP221 peptides, mouse CaM, and Pcdp1

RT-PCR was used to generate cDNA encoding FAP221 aa 554–668 that was ligated into the pCR2.1 vector (Invitrogen) after being PCR amplified. Primers were then used to PCR amplify two products from this vector: the first spanning the region encoding aa 554–611, and the second region encoding aa 606–668. The resulting PCR products were first ligated into the PCR2.1 vector using the TOPO-TA cloning kit (Invitrogen). The PCR fragments were then shuttled into the pET30B and pET30A expression vectors, respectively (EMD). The constructs were transformed into BL21 (DE3) pLysS cells (EMD). Expression was induced by the addition of IPTG to a final concentration of 2 mM. The protein was isolated and purified using the manufacturer's denaturing protocol. Peak fractions were dialyzed against 2M urea in PBS, fixed with SDS sample buffer, and run on SDS-polyacrylamide gels.

For expression of mouse proteins, first PCR was performed using cDNA from mouse testes (Ernst Laboratory, Dartmouth College, Hanover, NH) as a template. Primers were designed based on the published protein-coding sequences. PCR products were cloned into the pCR2.1 vector using the TOPO-TA cloning kit (Invitrogen). The PCR products were then shuttled into the pET30 series of expression vectors (EMD) and purified as above. The entire mouse CaM coding sequence was expressed in pET30A. Two regions of Pcdp1 were expressed: Pcdp1-1 spanning aa 791–8836 in pET30C and Pcdp1-2 spanning aa 447–530 in pET30A.

Site-directed mutagenesis

The FAP221 CaM-binding site is encoded by aa 588–595. RT-PCR was used to generate a cDNA fragment encoding aa 554–668. After PCR amplification, this fragment was ligated into the PCR2.1 vector. Site-directed mutagenesis was performed as described in the Stratagene QuikChange XL site-directed mutagenesis protocol. Primers HC4-CaM-For

(5′-GGTGGTGACGCACCAGCGCCAGCAGCAGCAGCTGG-3′) and HC4-CaM-Rev (5′-CCAGCTGCTGCTGCTGGCGCTGGTGCGTCACCACC-3′) were designed to alter aa 592 (leucine), 594 (arginine), and 595 (arginine) to glutamines by altering a single nucleotide base in each codon. Site-directed mutagenesis was achieved by PCR amplification of the cDNA fragment with the above primers using a specific PCR program designed as per the manufacturer's instructions. DpnI was added to the finished PCR reaction, which digests the methylated plasmid template. The digested PCR reaction was then transformed into *Escherichia coli* cells (TOP10). Sequencing of miniprepped plasmids confirmed the incorporation of the nucleotide base pair changes. The FAP221 fragment containing the altered CaM-binding site was then ligated into pET30B and transformed into BL21 (DE3) pLysS cells (EMD). Induction and purification were performed as described above.

Gels, blots, and blot overlays

Gel electrophoresis, silver staining, and Western blots were preformed as described previously (Dymek and Smith, 2007). Serum antibodies were used at a 1:1,000 (FAP221), 1:5,000 (FAP74), or 1:7,000 (CaM) dilution in TBS-T. For FAP221 and FAP74 blots, 2% nonfat dry milk was added to the TBS-T during primary and secondary incubations.

Blot overlays were performed as described previously (Dymek and Smith, 2007) with the following modifications. CaM::6XHis protein for blot overlays was isolated from bacteria using a phenylsepharose column according to the manufacturer's instructions (GE Healthcare). CaM::6XHis protein was diluted to a concentration of 10 µg/ml in TBS-T with 1% BSA and either 0.1mM $CaCl_2$ or 5.0 mM EDTA and incubated with the membrane for 2 h at room temperature. After three 5 min TBS-T washes, membranes were blocked again in 5% milk in TBS-T. After a quick TBS-T wash, blots were incubated with a CaM antibody at 1:7,000 in TBS-T for 1 h. After three 5 min TBS-T washes, membranes were incubated in HRP-conjugated donkey anti–rabbit IgG (GE Healthcare) diluted 1:30,000 in TBS-T for 30 min.

For CaM overlays using mouse CaM, the purified protein was biotinylated with the EZ-link Sulfo-NHS-LC-Biotinylation kit from Thermo Fisher Scientific as per the manufacturer's instructions. The biotinylated CaM was then detected with streptavidin-HRP (GE Healthcare) followed by visualization by ECL+ (GE Healthcare).

Mass spectrometry, RNA isolation, and RT-PCR

High calcium anti-CaM immunoprecipitation from *pf14* NaCl axonemal extracts was performed as described above. Proteins precipitated from 600 µg of axonemal extract were eluted in a final volume of 90 µl of TBS-T in order to concentrate the sample and loaded onto a large-frame 5% polyacrylamide gel. Gels were run at 11 V for 18 h and Coomassie stained. Protein bands were extracted and analyzed by MALDI-TOF (matrix-assisted laser desorption/ionization-time of flight) mass spectrometry with PSD (post-source decay) conducted at the University of Massachusetts Medical School (Worcester, MA) or at Dartmouth College (Hanover, NH). Comparisons of peptide masses with translated genomic or EST sequences were made using the *C. reinhardtii* genome database (http://genome.jgi-psf.org/Chlre3/Chlre3.home.html). The complete coding sequences for FAP74 and FAP221 were confirmed by RT-PCR performed as described previously (Dymek and Smith, 2007). PCR primers were designed based on the predicted coding regions published in the *C. reinhardtii* genome database or GreenGenie2 coding sequence prediction software (Kwan et al., 2009). Complete coding sequences were deposited into the National Center for Biotechnology Information (NCBI) for FAP221 (accession no. 1313266) and FAP74 (accession no. 1313270).

Construction of expression vectors, antibody production, and affinity purification

Polyclonal antibodies for FAP221 were generated in rabbits against bacterially expressed proteins. RT-PCR was used to generate cDNA encoding aa 403–771. The amplified PCR product was ligated into the PCR2.1 vector using the TOPO-TA cloning kit (Invitrogen). Two tandem PCR fragments were then shuttled into the pET30A expression vector (EMD). Orientation and reading frame were confirmed by DNA sequencing. The construct was transformed into BL21 (DE3) pLysS cells (EMD) and expression was induced using 2 mM IPTG. Protein was purified on a Ni^{2+}-resin column according to the manufacturer's instructions. Peak fractions were dialyzed against 2.0M urea in PBS, fixed with SDS sample buffer, and subjected to SDS-PAGE. Protein bands were excised from Coomassie-stained gels and used for polyclonal antibody production in rabbits. Rabbits were injected twice with 300 µg of protein per injection. Antibody production was conducted by Spring Valley Laboratories, Inc.

Polyclonal antibodies for FAP74 were generated in rabbits against synthetic peptides corresponding to aa 41–56 (N-terminal) and 1894–1909 (C-terminal). Each synthetic peptide had a cysteine added to the C-terminal end and was conjugated to KLH before being used for antibody production by Spring Valley Laboratories, Inc. Both the N- and C-terminal synthetic peptides were co-injected into rabbits for antibody production. The remaining synthetic peptides were conjugated to Sulfolink resin (Thermo Fisher Scientific) according to the manufacturer's instructions to prepare separate N- and C-terminal antigen-specific affinity columns. Affinity-purified N-terminal–derived antibody was used for anti-FAP74 immunoprecipitation.

The initial studies for this manuscript used anti–*C. reinhardtii* CaM antibodies that we generated as described previously (Wargo et al., 2005). Our supply of this antibody was exhausted part way through these studies. Therefore, we generated additional anti-CaM antibodies using the same synthetic peptide (RMMTSGATDDKDKKGHK) and methods as described in Wargo et al. (2005).

amiRNA construct, transformation, and screening

pChlamiRNA3int was obtained from the *Chlamydomonas* Resource Center at the University of Minnesota (St. Paul, MN). The sequence and vector map can be downloaded from the Baulcombe laboratory website (http://www.plantsci.cam.ac.uk/research/baulcombe/sequencedata.html). pChlamiRNA3int contains the precursor for cre-MIR1157 as an artificial miRNA template and the aphVIII gene for selection. We followed the protocols in Ossowski et al. (2008) and Molnar et al. (2009) (see also Zhao et al., 2008). Potential FAP74 amiRNA target sequences were identified using the Web MicroRNA Designer platform (WMD2; http://wmd2.weigelworld.org/cgi-bin/mirnatools.pl). The amiRNA sequence (5′-TAAGTCATGAGGTGAGCCGTG-3′) was chosen to target FAP74 coding sequence for nucleotides 2298–2317 (5′-CATGGCTCACCTCATGACTT-3′). The amiRNA sequence was used to design forward and reverse oligonucleotides consisting of the target sequence, followed by a spacer region and the amiRNA sequence, and SpeI sequences on both ends. The annealed target gene–specific oligonucleotides were ligated into the SpeI-digested pChlamiRNA3int to produce pChlamiRNA3int-FAP74. Bacterial transformants were screened by colony PCR to confirm the correct orientation of the insert using forward primer 5′-GGTGTTTGGGTCGGTGTTTTTG-3′ and reverse primer 5′-TAGCGCTGATCACCACCACCC-3′. Isolated plasmids were transformed into A54-e18 *C. reinhardtii* cells by the glass beads method (Kindle, 1990). Transformants were selected on TAP plates containing 10 µg/ml paromomycin. Colonies were picked into 96-well dishes filled with TAP media and screened for swimming defects using a stereoscope. Flagella isolated from potential amiRNA mutants were screened by Western blot for the presence of FAP74. Densitometry was performed using ImageQuant software (GE Healthcare).

Southern and Northern blots

Southern blotting using the aphVIII gene as probe confirmed that integration of the plasmid occurred randomly in the genomes of the three transformants selected for further analysis (Fig. S2). Reduced expression of FAP74 was also confirmed by Northern blot using the FAP74 gene as a probe. For Southern blots, 20 µg of genomic DNA was digested with NotI, fractionated on a 1% agarose gel, and transferred to MagnaGraph nylon membrane (GE Healthcare). The membrane was washed in prehybridization solution (5x SSPE, 10x Denhardt's, 1% SDS, and 300 µg/ml salmon sperm DNA) for 3 h at 65°C. The aphVIII gene was labeled with a random primed DNA labeling kit (Roche) using 50 µCi α-[^{32}P]dCTP according to the manufacturer's instructions, added to prehybridization solution, and allowed to hybridize to the membrane for 16 h at 65°C. After extensive washing, the membrane was exposed on a phosphor screen for 6 h. The phosphor screen was then scanned with a Typhoon 9200 Imager (GE Healthcare).

For Northern blots, total RNA was isolated from cells at 0 and 45 min after deflagellation. 50 µg of total RNA was fractionated on a 1% agarose gel containing formaldehyde and transferred to Hybond-N+ nylon membrane (GE Healthcare). The membrane was washed in prehybridization solution (5x SSPE, 0.5% SDS, 5x Denhardt's, and 100 µg/ml salmon sperm DNA) for 30 min at 65°C. FAP74 coding sequences representing aa 377–606, 741–963, and 1776–1940 were PCR amplified. Approximately 100 ng of each PCR product was labeled with a random primed DNA labeling kit (Roche) using 50 µCi α-[^{32}P]dCTP. The labeled probes were added to prehybridization solution and allowed to hybridize to the membrane for 16 h at 65°C. The membrane was then washed and treated as described in the Southern blot procedure. The *S14* gene encoding the ribosomal S14 protein served as a loading control.

Analysis of flagellar beat frequency, swimming velocity, and swimming behavior

High speed video microscopy was performed at room temperature using a MotionProY3 camera (Integrated Design Tools) at 500 fps using phase-contrast optics and a 40x objective with 0.65 NA on a microscope (Axioskop 2; Carl Zeiss, Inc.). Images were recorded as 8 bit with a 640 x 480 pixel resolution using Motion Studio software (Integrated Design Tools). A red filter was used during asymmetric waveform video recordings to prevent photoshock. To induce waveform conversion, the red filter was removed during video recording. Both beat frequency and swimming velocity were measured manually and statistical significance was determined using a Student's *t* test. Beat frequency and swimming velocity data were graphed using Excel (Microsoft) and proved to have a normal distribution. For Fig. 5, individual images were assembled into a montage and brightness and contrast were uniformly adjusted for all images using Photoshop (Adobe) to improve visibility of the flagella. Manual traces of flagellar position over successive images were overlapped to determine asymmetric waveform. The ability of FAP74ami transformants to phototax was assessed by covering a Petri dish filled with cells with a black plastic bag, leaving only a small edge exposed to the light. The cells were checked at 10-min intervals to see if photo-accumulation had occurred at the exposed edge of the dish.

Electron microscopy

For analysis of flagellar defects, axonemes from WT and mutants of interest were prepared for thin-section electron microscopy. Specimens were fixed with 1% glutaraldehyde and 1% tannic acid in 0.1 M sodium cacodylate, postfixed in 1% osmium tetroxide, dehydrated in a graded series of ethanol, and embedded in LX112 resin. Uniform silver-gray sections were mounted on Formvar-coated, carbon-stabilized copper grids, stained with uranyl acetate and Reynolds lead citrate, and examined at 100 kV in a transmission electron microscope (model 100CX; JEOL Ltd.) with side-mount 2K X2K ATM camera.

Online supplemental material

Fig. S1 shows a phylogenetic tree constructed using the results from BLAST searches with the FAP221 amino acid sequence. Fig. S2 includes both Southern and Northern blot analyses of FAP74 amiRNA transformants. We also include six movies. Video 1 shows swimming behavior of wild-type cells. Videos 2–4 demonstrate abnormal motility of FAP74 amiRNA transformants 1G11, 2D4, and 7A4, respectively. Video 5 demonstrates flagellar waveform conversion for wild-type cells. Video 6 demonstrates the inability of the FAP74ami transformant 1G11 to convert to a symmetric flagellar waveform. Online supplemental material is available at http://www.jcb.org/cgi/content/full/jcb.200912009/DC1.

We thank L. Howard (Dartmouth College, Hanover, NH) for expert technical assistance with electron microscopy and A. Lavanway (Dartmouth College, Hanover, NH) for technical assistance with high speed video recording.

This work was supported by NIH grant GM66919 (E.F. Smith) and NIH training grant 2-T32-GM008704 (C.G. DiPetrillo).

Submitted: 1 December 2009
Accepted: 5 April 2010

References

Badano, J.L., N. Mitsuma, P.L. Beales, and N. Katsanis. 2006. The ciliopathies: an emerging class of human genetic disorders. *Annu. Rev. Genomics Hum. Genet.* 7:125–148. doi:10.1146/annurev.genom.7.080505.115610

Bannai, H., M. Yoshimura, K. Takahashi, and C. Shingyoji. 2000. Calcium regulation of microtubule sliding in reactivated sea urchin sperm flagella. *J. Cell Sci.* 113:831–839.

Bessen, M., R.B. Fay, and G.B. Witman. 1980. Calcium control of waveform in isolated flagellar axonemes of *Chlamydomonas*. *J. Cell Biol.* 86:446–455. doi:10.1083/jcb.86.2.446

Brokaw, C.J., R. Josslin, and L. Bobrow. 1974. Calcium ion regulation of flagellar beat symmetry in reactivated sea urchin spermatozoa. *Biochem. Biophys. Res. Commun.* 58:795–800. doi:10.1016/S0006-291X(74)80487-0

Chin, D., and A.R. Means. 2000. Calmodulin: a prototypical calcium sensor. *Trends Cell Biol.* 10:322–328. doi:10.1016/S0962-8924(00)01800-6

DiPetrillo, C., and E.F. Smith. 2009. Calcium regulation of ciliary motility: analysis of axonemal calcium binding proteins. *In* Methods in Cell Biology. Vol. 92 Cilia: Motors and Regulation. S.J. King and G.J. Pazour, editors. Elsevier, St. Louis. 163–180.

Dutcher, S.K., B. Huang, and D.J. Luck. 1984. Genetic dissection of the central pair microtubules of the flagella of *Chlamydomonas reinhardtii*. *J. Cell Biol.* 98:229–236. doi:10.1083/jcb.98.1.229

Dymek, E.E., and E.F. Smith. 2007. A conserved CaM- and radial spoke associated complex mediates regulation of flagellar dynein activity. *J. Cell Biol.* 179:515–526. doi:10.1083/jcb.200703107

Frey, E., C.J. Brokaw, and C.K. Omoto. 1997. Reactivation at low ATP distinguishes among classes of paralyzed flagella mutants. *Cell Motil. Cytoskeleton.* 38:91–99. doi:10.1002/(SICI)1097-0169(1997)38:1<91::AID-CM8>3.0.CO;2-K

Gorman, D.S., and R.P. Levine. 1965. Cytochrome f and plastocyanin: their sequence in the photosynthetic electron transport chain of *Chlamydomonas reinhardi*. *Proc. Natl. Acad. Sci. USA.* 54:1665–1669. doi:10.1073/pnas.54.6.1665

Hayashi, S., and C. Shingyoji. 2009. Bending-induced switching of dynein activity in elastase-treated axonemes of sea urchin sperm—roles of Ca2+ and ADP. *Cell Motil. Cytoskeleton.* 66:292–301. doi:10.1002/cm.20360

Kindle, K.L. 1990. High-frequency nuclear transformation of *Chlamydomonas reinhardtii*. *Proc. Natl. Acad. Sci. USA.* 87:1228–1232. doi:10.1073/pnas.87.3.1228

Kwan, A.L., L. Li, D.C. Kulp, S.K. Dutcher, and G.D. Stormo. 2009. Improving gene-finding in *Chlamydomonas reinhardtii*:GreenGenie2. *BMC Genomics.* 10:210. doi:10.1186/1471-2164-10-210

Lechtreck, K.F., and G.B. Witman. 2007. *Chlamydomonas reinhardtii* hydin is a central pair protein required for flagellar motility. *J. Cell Biol.* 176:473–482. doi:10.1083/jcb.200611115

Lechtreck, K.F., P. Delmotte, M.L. Robinson, M.J. Sanderson, and G.B. Witman. 2008. Mutations in Hydin impair ciliary motility in mice. *J. Cell Biol.* 180:633–643. doi:10.1083/jcb.200710162

Lee, L., D.R. Campagna, J.L. Pinkus, H. Mulhern, T.A. Wyatt, J.H. Sisson, J.A. Pavlik, G.S. Pinkus, and M.D. Fleming. 2008. Primary ciliary dyskinesia in mice lacking the novel ciliary protein Pcdp1. *Mol. Cell. Biol.* 28:949–957. doi:10.1128/MCB.00354-07

Merchant, S.S., S.E. Prochnik, O. Vallon, E.H. Harris, S.J. Karpowicz, G.B. Witman, A. Terry, A. Salamov, L.K. Fritz-Laylin, L. Maréchal-Drouard, et al. 2007. The *Chlamydomonas* genome reveals the evolution of key animal and plant functions. *Science.* 318:245–250. doi:10.1126/science.1143609

Mitchell, D.R. 2009. The flagellar central pair apparatus. *In* The *Chlamydomonas* Sourcebook. Vol. Volume 3: Cell Motility and Behavior. G.B. Witman, editor. Elsevier, New York. 235-248.

Mitchell, D.R., and M. Nakatsugawa. 2004. Bend propagation drives central pair rotation in *Chlamydomonas reinhardtii* flagella. *J. Cell Biol.* 166:709–715. doi:10.1083/jcb.200406148

Mitchell, D.R., and W.S. Sale. 1999. Characterization of a *Chlamydomonas* insertional mutant that disrupts flagellar central pair microtubule-associated structures. *J. Cell Biol.* 144:293–304. doi: 10.1083/jcb.144.2.293

Molnar, A., A. Bassett, E. Thuenemann, F. Schwach, S. Karkare, S. Ossowski, D. Weigel, and D. Baulcombe. 2009. Highly specific gene silencing by artificial microRNAs in the unicellular alga *Chlamydomonas reinhardtii*. *Plant J.* 58:165–174. doi:10.1111/j.1365-313X.2008.03767.x

Nakano, I., T. Kobayashi, M. Yoshimura, and C. Shingyoji. 2003. Central-pair-linked regulation of microtubule sliding by calcium in flagellar axonemes. *J. Cell Sci.* 116:1627–1636. doi:10.1242/jcs.00336

Nigg, E.A., and J.W. Raff. 2009. Centrioles, centrosomes, and cilia in health and disease. *Cell.* 139:663–678. doi:10.1016/j.cell.2009.10.036

Omoto, C.K., T. Yagi, E. Kurimoto, and R. Kamiya. 1996. Ability of paralyzed flagella mutants of *Chlamydomonas* to move. *Cell Motil. Cytoskeleton.* 33:88–94. doi:10.1002/(SICI)1097-0169(1996)33:2<88::AID-CM2>3.0.CO;2-E

Ossowski, S., R. Schwab, and D. Weigel. 2008. Gene silencing in plants using artificial microRNAs and other small RNAs. *Plant J.* 53:674–690. doi:10.1111/j.1365-313X.2007.03328.x

Patel-King, R.S., S.E. Benashski, and S.M. King. 2002. A bipartite Ca2+-regulated nucleoside-diphosphate kinase system within the *Chlamydomonas* flagellum. The regulatory subunit p72. *J. Biol. Chem.* 277:34271–34279. doi:10.1074/jbc.M204137200

Patel-King, R.S., O. Gorbatyuk, S. Takebe, and S.M. King. 2004. Flagellar radial spokes contain a Ca2+-stimulated nucleoside diphosphate kinase. *Mol. Biol. Cell.* 15:3891–3902. doi:10.1091/mbc.E04-04-0352

Pazour, G.J., N. Agrin, J. Leszyk, and G.B. Witman. 2005. Proteomic analysis of a eukaryotic cilium. *J. Cell Biol.* 170:103–113. doi:10.1083/jcb.200504008

Rupp, G., E. O'Toole, and M.E. Porter. 2001. The *Chlamydomonas* PF6 locus encodes a large alanine/proline-rich polypeptide that is required for assembly of a central pair projection and regulates flagellar motility. *Mol. Biol. Cell.* 12:739–751.

Sharma, N., N.F. Berbari, and B.K. Yoder. 2008. Ciliary dysfunction in developmental abnormalities and diseases. *Curr. Top. Dev. Biol.* 85:371–427. doi:10.1016/S0070-2153(08)00813-2

Smith, E.F. 2002. Regulation of flagellar dynein by calcium and a role for an axonemal calmodulin and calmodulin-dependent kinase. *Mol. Biol. Cell.* 13:3303–3313. doi:10.1091/mbc.E02-04-0185

Smith, E.F., and P. Yang. 2004. The radial spokes and central apparatus: mechano-chemical transducers that regulate flagellar motility. *Cell Motil. Cytoskeleton.* 57:8–17. doi:10.1002/cm.10155

Verdugo, P. 1980. Ca2+-dependent hormonal stimulation of ciliary activity. *Nature.* 283:764–765. doi:10.1038/283764a0

Wakabayashi, K., T. Yagi, and R. Kamiya. 1997. Ca2+-dependent waveform conversion in the flagellar axoneme of *Chlamydomonas* mutants lacking the central-pair/radial spoke system. *Cell Motil. Cytoskeleton.* 38:22–28. doi:10.1002/(SICI)1097-0169(1997)38:1<22::AID-CM3>3.0.CO;2-J

Wargo, M.J., and E.F. Smith. 2003. Asymmetry of the central apparatus defines the location of active microtubule sliding in *Chlamydomonas* flagella. *Proc. Natl. Acad. Sci. USA.* 100:137–142. doi:10.1073/pnas.0135800100

Wargo, M.J., M.A. McPeek, and E.F. Smith. 2004. Analysis of microtubule sliding patterns in *Chlamydomonas* flagellar axonemes reveals dynein activity on specific doublet microtubules. *J. Cell Sci.* 117:2533–2544. doi:10.1242/jcs.01082

Wargo, M.J., E.E. Dymek, and E.F. Smith. 2005. Calmodulin and PF6 are components of a complex that localizes to the C1 microtubule of the flagellar central apparatus. *J. Cell Sci.* 118:4655–4665. doi:10.1242/jcs.02585

Yagi, T., and R. Kamiya. 2000. Vigorous beating of *Chlamydomonas* axonemes lacking central pair/radial spoke structures in the presence of salts and organic compounds. *Cell Motil. Cytoskeleton.* 46:190–199. doi:10.1002/1097-0169(200007)46:3<190::AID-CM4>3.0.CO;2-#

Yang, P., D.R. Diener, J.L. Rosenbaum, and W.S. Sale. 2001. Localization of calmodulin and dynein light chain LC8 in flagellar radial spokes. *J. Cell Biol.* 153:1315–1326. doi:10.1083/jcb.153.6.1315

Yoshimura, M., and C. Shingyoji. 1999. Effects of the central pair apparatus on microtubule sliding velocity in sea urchin sperm flagella. *Cell Struct. Funct.* 24:43–54. doi:10.1247/csf.24.43

Zhao, T., W. Wang, X. Bai, and Y. Qi. 2008. Gene silencing by artificial microRNAs in *Chlamydomonas*. *Plant J.* 58:157–164. doi:10.1111/j.1365-313X.2008.03758.x